

# Effect of In-Incorporation and Annealing on Cu<sub>x</sub>Se Thin Films

Algimantas Ivanauskas, Remigijus Ivanauskas \* and Ingrida Ancutiene

Department of Physical and Inorganic Chemistry, Faculty of Chemical Technology, Kaunas University of Technology, 44249 Kaunas, Lithuania; algimantas.ivanauskas.88@gmail.com (A.I.); ingrida.ancutiene@ktu.lt (I.A.)

\* Correspondence: remigijus.ivanauskas@ktu.lt; Tel.: +370-605-680-35

**Abstract:** A study of indium-incorporated copper selenide thin-film deposition on a glass substrate using the successive ionic adsorption and reaction method (SILAR) and the resulting properties is presented. The films were formed using these steps: selenization in the solution of diseleniumtetrathionate acid, treatment with copper(II/I) ions, incorporation of indium(III), and annealing in an inert nitrogen atmosphere. The elemental and phasal composition, as well as the morphological and optical properties of obtained films were determined. X-ray diffraction data showed a mixture of various compounds: Se, Cu<sub>0.87</sub>Se, In<sub>2</sub>Se<sub>3</sub>, and CuInSe<sub>2</sub>. The obtained films had a dendritic structure, agglomerated and not well-defined grains, and a film thickness of ~90 μm. The band gap values of copper selenide were 1.28–1.30 eV and increased after indium-incorporation and annealing. The optical properties of the formed films correspond to the optical properties of copper selenide and indium selenide semiconductors.

**Keywords:** SILAR; selenium; copper selenide; indium selenide



**Citation:** Ivanauskas, A.; Ivanauskas, R.; Ancutiene, I. Effect of In-Incorporation and Annealing on Cu<sub>x</sub>Se Thin Films. *Materials* **2021**, *14*, 3810. <https://doi.org/10.3390/ma14143810>

Academic Editors: Victor Leca and Maria Dinescu

Received: 28 May 2021

Accepted: 2 July 2021

Published: 8 July 2021

**Publisher's Note:** MDPI stays neutral with regard to jurisdictional claims in published maps and institutional affiliations.



**Copyright:** © 2021 by the authors. Licensee MDPI, Basel, Switzerland. This article is an open access article distributed under the terms and conditions of the Creative Commons Attribution (CC BY) license (<https://creativecommons.org/licenses/by/4.0/>).

## 1. Introduction

While the majority of the world's energy supply is generated from non-renewable fossil fuels, such as oil, coal, and natural gas, there are a number of disadvantages in using them, such as rising prices, increasing environmental concerns over climate change, and security concerns due to dependency on imports from a limited number of countries that have substantial fossil fuel supplies. As a result, governments and businesses increasingly support renewable energies such as wind, hydroelectric, geothermal, biomass, and solar power.

Solar power is proven to be one of the most promising and popular renewable energy sources today since it has several advantages over other renewable energy sources. Solar power generates energy with very limited environmental impact. Its peak energy output matches the peak energy demand time, making it a perfect supplement for already existing power grids. Solar power plants are very easy to scale up, as the energy generating capacity is directly dependent on the plant's size and the number of modules installed. Solar power production facilities can be installed in environmentally sensitive and remote locations, such as national parks and remote homes, where no power grid and other energy sources are available. Solar cells have no moving parts, thus they require little service and operate noise free. The worldwide production of solar power has been increasing exponentially during the last decades [1].

Copper indium selenide is a widely used thin-film substance in solar energy and photovoltaic applications. Over the years, it has attracted a lot of attention due to its desired physical properties. CuInSe<sub>2</sub> has a low direct band gap (1.04 eV) [2], a high absorption coefficient (>10<sup>5</sup> cm<sup>-1</sup>) [2], and a high thermal resilience [3]. It shows no performance degradation under intensive solar radiation [4]. Currently, maximum CuInSe<sub>2</sub> efficiencies of 23.3% were achieved in thin-film layers, and 22.9% in solar cells [5]. Due to continuous improvements in the efficiency of CuInSe<sub>2</sub> cells, it is now widely used in photovoltaic technologies.

CuInSe<sub>2</sub> films can be formed using various deposition methods. Chemical deposition methods include spin-coating [6], electrochemical deposition [7], and chemical bath deposition [8], while physical deposition methods include electron beam evaporation [9], sputtering [10], molecular beam epitaxy [11], physical vapor deposition [12], printing [13], etc. Films which are formed using physical deposition methods are usually more uniform and of better quality; however, expensive, high-temperature, and low-pressure equipment is often needed. Furthermore, these methods offer low scalability for large-area coating and often require a toxic H<sub>2</sub>Se atmosphere to anneal. This results in a toxic work environment and lower cost efficiency due to wasted reagents. Chemical deposition methods are a more convenient way to deposit CuInSe<sub>2</sub>, due to not needing hazardous selenization processes and not requiring expensive instrumentation. In addition, it is much easier to make films with a large surface area. Thus, two wet chemical deposition methods, such as chemical bath deposition (CBD) [14,15] and successive ionic layer adsorption and reaction (SILAR) [16,17], are widely studied and used to deposit thin semiconductor films on various substrates. However, one of the drawbacks of the CBD method is the waste of the solution after each deposition. This also leads to the formation of a precipitate in the solution and complications in controlling the process. By using the SILAR method, thin-film deposition occurs by contacting the substrate with a chemical bath containing the appropriate ions, thus avoiding the formation of precipitate. D. Kishore Kumar et al. have shown [18] that the SILAR method provides phase purity of a tin selenide layer formed and used in solar cells. In addition, this method allows the thickness, morphology, and composition to be controlled, which is very important for the optical properties of a thin film [19].

The films formed using chemical deposition methods often require annealing to obtain a crystalline layer and improve properties.

The incorporation of elements has been found to be an effective way to modify the properties of semiconductors and improve the conversion efficiency of solar energy. Indium is considered to be one of the most efficient elements that can be used to improve the conductivity of thin films.

This work studies the deposition of In-incorporated Cu<sub>x</sub>Se films on a glass substrate using the three-step SILAR method and subsequent annealing in a nitrogen atmosphere. To understand the reaction pathways, composition, and properties of obtained films, X-ray diffraction (XRD), X-ray photoelectron spectroscopy (XPS), scanning electron microscopy (SEM), energy dispersive X-ray spectroscopy (EDX), atomic absorption spectroscopy (AAS), and ultraviolet-visible spectroscopy (UV-Vis) measurements were carried out.

## 2. Materials and Methods

### 2.1. Materials

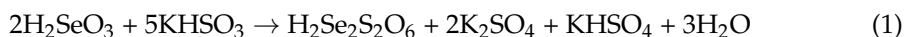
All chemicals used are pure commercial reagents from Sigma–Aldrich (Sigma-Aldrich Chemie GmbH, Taufkirchen, Germany): KHSO<sub>3</sub> (≥98.0%), H<sub>2</sub>SeO<sub>3</sub> (99.99% trace metals basis), CuSO<sub>4</sub>·5H<sub>2</sub>O (99.99% crystals and lumps), hydroquinone (≥99% flakes), and InCl<sub>3</sub> (98% reagent grade).

Thomas<sup>®</sup> environmental glass slides with one side sandblasted (20 × 20 mm<sup>2</sup>) were used for film deposition.

### 2.2. Treatment Methods

Before the thin-film deposition process, glass slides were thoroughly cleaned with liquid soap, washed with distilled water, and then bathed ultrasonically in acetone using the Sonoswiss SW 3 H cleaner in sweep mode at 40 °C for 10 min. After cleaning, glass slides were dried before use.

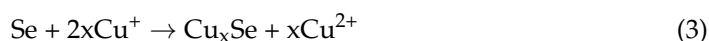
In-incorporated  $\text{Cu}_x\text{Se}$  films were deposited in three stages and then annealed. The first step was selenization at 60 °C for 180 min in diseleniumtetrathionate acid solution, which is produced by mixing of 1 mol/L  $\text{KHSO}_3$  and 0.4 mol/L  $\text{H}_2\text{SeO}_3$  (1:1) [20]:



Elemental selenium is deposited by submerging glass substrate into  $\text{H}_2\text{Se}_2\text{S}_2\text{O}_6$  solution, which decomposes into elemental selenium and seleniumtrithionate via reaction (2) [21]:



The deposited selenium film was washed in distilled water, and then submerged in copper(II/I) ion solution at 40 °C for 10 or 20 min, and 60 °C for 5 or 10 min. Cu(II/I) salt solution was prepared using a solution of 0.4 mol/L  $\text{CuSO}_4$  and a reducing agent, hydroquinone (1%), therefore being a mixture of univalent and divalent copper salts. Cu(I) ions react with elemental selenium forming copper selenide via reaction (3):



Copper selenide films were washed in distilled water and then treated with 0.1 mol/L  $\text{InCl}_3$  solution at 40 °C for 20 min. Obtained films were washed again in distilled water and dried over  $\text{CaCl}_2$ . The final step was film annealing at 100 °C for 12 h in an inert  $\text{N}_2$  atmosphere. The deposition scheme is shown in Figure 1.

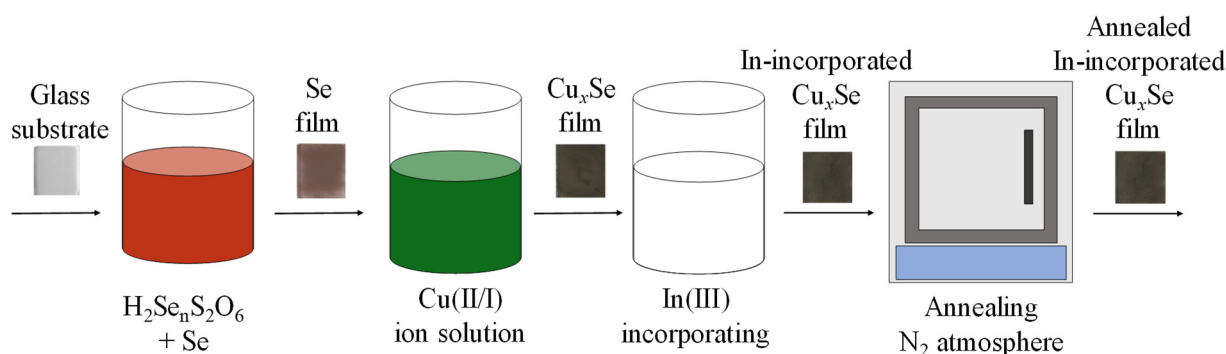


**Figure 1.** Schematic representation of In-incorporated  $\text{Cu}_x\text{Se}$  film on glass synthesis.

### 2.3. Investigative Methods

X-ray diffraction analysis was conducted with a D8 Advance diffractometer (Bruker AXS, Karlsruhe, Germany) at 40 mA tube current and 40 kV voltage. 6° 1/min scanning speed was used with coupled two theta/theta scan type. Data was recorded with provided software package DIFFRAC.SUITE (Diffract.EVA.V4.3., Bruker, Karlsruhe, Germany) and analyzed using Search Match and Microsoft Office Excel.

X-ray photoelectron spectroscopy analysis was made using the upgraded Vacuum Generator (VG) ESCALAB MKII spectrometer (Waltham, MA, USA), with an added XR4 twin anode. Thermo VG Scientific Advantage software (5.918, Thermo Fisher Scientific, Waltham, MA, USA) was used to record data. Data were analyzed in Microsoft Office Excel.

Scanning electron microscopy analysis of In-incorporated  $\text{Cu}_x\text{Se}$  film morphology was carried out with a Quanta 200 FEG microscope. Bruker XFlash 4030 detector (Bruker Corporation, Billerica, MA, USA) was used to perform energy dispersive X-ray analysis. Detected elements were quantified using ZAF method.

Atomic absorption spectroscopy analysis by atomic absorption spectrometer Shimadzu AA-7000 (Tokyo, Japan) was used to determine Se, Cu, and In amounts in In-incorporated  $\text{Cu}_x\text{Se}$  films deposited on glass. A mixture of concentrated  $\text{HNO}_3$  and

distilled water (1:1) was used to dissolve films. Acetylene–air combination was used as flame fuel. Amount ( $\mu\text{mol}/\text{cm}^2$ ) of Se, Cu, In in film was calculated using measured data.

To measure optical absorption spectra of 400–900 nm, Perkin Elmer Lambda 35 UV/VIS (Waltham, MA, USA) spectrometer with fitted diffuse reflectance sphere Lab-sphere RSA-PE-20 was used. Band gap  $E_g$  was calculated by plotting  $(\alpha h\nu)^2$  against photon energy  $h\nu$ , extrapolating linear part of the plot until abscissa axis intersection ( $(\alpha h\nu)^2 = 0$ ). Then, band gap value  $E_g$  was equal to  $h\nu$  at intersected part.

### 3. Results and Discussion

XRD, XPS, SEM/EDX, and AAS analyses were used in order to better understand the reaction pathways when using the SILAR deposition method, and to learn more about film composition during various formation steps.

#### 3.1. XRD Analysis

Copper selenide and indium-incorporated  $\text{Cu}_x\text{Se}$  films were formed on a glass substrate with a single-side matte finish. Figure 2 shows the XRD patterns of selenide films on glass for various formation stages. Graph (a) shows XRD patterns after the treatment of selenium films in copper(II/I) ion solution. Here, four peaks of hexagonal klockmannite  $\text{Cu}_{0.87}\text{Se}$  ( $\diamond$ ) at  $2\theta = 26.6, 28.1, 31.2, 50.0^\circ$  (JCPDS: 83-1814) could be seen. Samples that were treated both longer (20 min vs. 10 min) and at higher temperature ( $60^\circ\text{C}$  vs.  $40^\circ\text{C}$ ) have slightly more intense peak values, indicating that more copper selenide was formed. This suggests that copper(I) ions react with elemental selenium, forming copper selenide as shown in Equation (3). Second graph (b) shows the XRD patterns after incorporation of indium(III). It could be seen from the graph that a brand-new peak of cubic indium selenide  $\text{In}_2\text{Se}_3$  at  $2\theta = 46.0^\circ$  (JCPDS: 20-492) appears in all XRD patterns. Indium(III) ions may react with copper selenide, forming indium selenide, according to reaction (4):

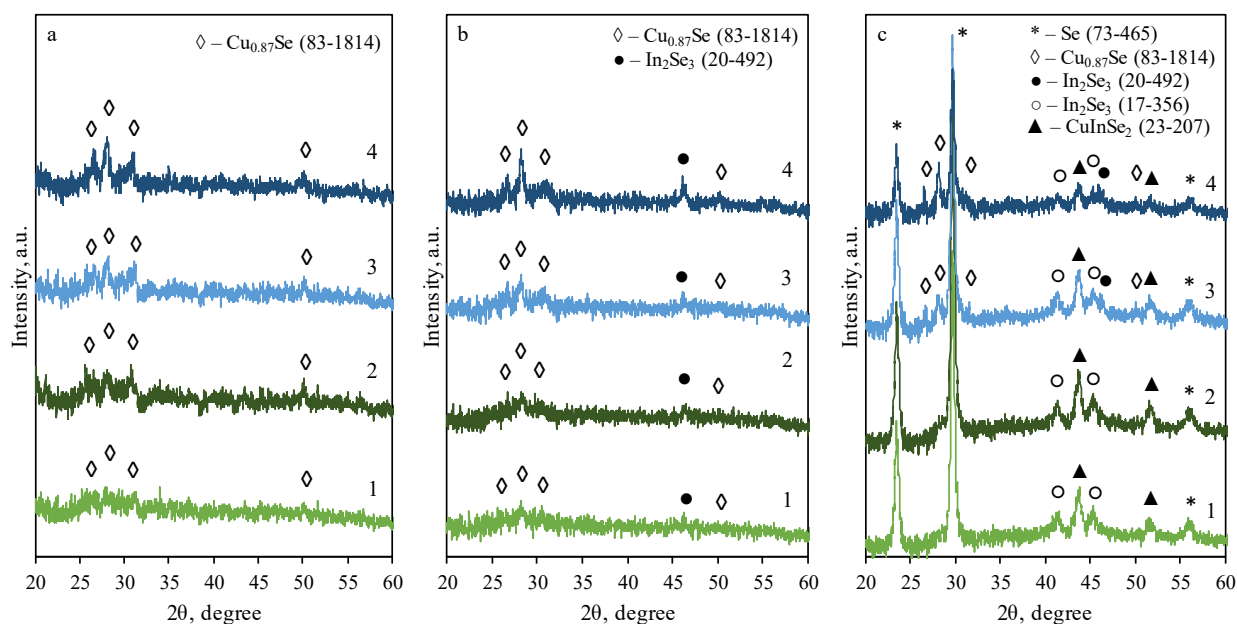
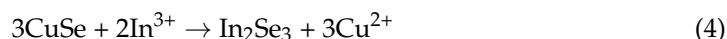
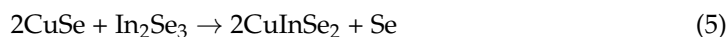


**Figure 2.** XRD patterns of  $\text{Cu}_x\text{Se}$  and In-incorporated  $\text{Cu}_x\text{Se}$  films on glass substrate: (a) treated with copper(II/I) ion solution, (b) treated with indium(III) salt solution, (c) annealed in nitrogen atmosphere. Treatment with copper(II/I) ion solution: 1—10 min at  $40^\circ\text{C}$ ; 2—20 min at  $40^\circ\text{C}$ ; 3—5 min at  $60^\circ\text{C}$ ; and 4—10 min at  $60^\circ\text{C}$ .

Ion exchange takes place due to the lower solubility of  $\text{In}_2\text{Se}_3$  (solubility product is  $5.6 \times 10^{-92}$ ) than of  $\text{CuSe}$  ( $1.4 \times 10^{-36}$ ) [22]. Similarly, samples that were treated longer and

with higher temperatures have slightly more intense peaks, indicating that more indium selenide was formed.

Finally, the samples were annealed in an inert nitrogen atmosphere at 100 °C to obtain better crystalline properties. Annealing promotes reactions between solid phases and crystallization of amorphous phases:



A number of new peaks can be seen in graph (c). Two intensive diffraction peaks at  $2\theta = 23.5, 29.7^\circ$  and one weaker peak at  $56.3^\circ$  of hexagonal selenium (JCPDS: 73-465) are clearly observed. Evidently, amorphous elemental selenium crystallized during the annealing process. Two new peaks at  $2\theta = 41.2, 45.3^\circ$  (JCPDS: 17-356) of the new phase of  $\text{In}_2\text{Se}_3$  indium selenide appear. The new phase may change the previous phase of cubic indium selenide due to annealing. This is suggested by the disappeared peaks of cubic indium selenide in samples 1 and 2 and the smaller peaks in 3 and 4, compared to graph (b). The other two new peaks of  $\text{CuInSe}_2$  cubic copper indium selenide phase at  $2\theta = 43.7, 51.8^\circ$  (JCPDS: 23-207) are found in the XRD patterns. A new phase of copper indium selenide may be formed during the solid phase reaction according to Equation (5). After annealing, the peaks of the hexagonal klockmannite phase are no longer found in samples 1 and 2. This could also be explained by Equation (5), as klockmannite was used in copper indium selenide formation.

### 3.2. XPS Analysis

The high-resolution XPS spectra are shown in Figure 3. Spectra were recorded at three regions corresponding to Se, Cu, and In. The data are presented in graph (a) for non-etched samples and in graph (b) for 30 s etched samples using an argon gas gun. Etching was necessary because the formed oxides, salt residues from solutions, and other residues could have been on the film surface.

Firstly, the glass substrate was submerged into a selenopolythionic acid solution and a reddish elemental selenium film was formed. The band gap of selenium film was 1.60 eV (Figure 6a) and corresponded to the values found in the literature. The band gap values of formed copper selenide films were in the range of 1.28–1.30 eV (Figure 6b) and are similar to the  $\text{Cu}_2\text{Se}$  band gap  $E_g = 1.1\text{--}1.27$  eV and  $\text{Cu}_{2-x}\text{Se}$  band gap  $E_g = 1.4\text{--}2.2$  eV (Table 2). After incorporation of In(III), the band gap values of those films increased to  $E_g = 1.32\text{--}1.38$  eV (Figure 6c). After annealing, the band gap values of films increased again to  $E_g = 1.44\text{--}1.48$  eV (Figure 6d). This is similar to the mixed phase of Cu-In-Se materials  $E_g = 1.17\text{--}1.24$  eV and to the band gap value of  $\text{In}_2\text{Se}_3$   $E_g = 1.55$  eV (Table 2). The annealing process allowed selenium to crystallize; therefore, the increase in band gap value could be due to the higher band gap value of selenium.

The peaks corresponding to the  $\text{Se}3d_{3/2}$  spectra region have binding energies of 55.5–55.8 eV. These peaks correspond to elemental-selenium-binding energy values of 55.7 eV [23]. The peaks in  $\text{Cu}2p_{1/2}$  and  $\text{Cu}2p_{3/2}$  regions are slightly more intense in samples treated with a solution of copper(II/I) ions at a higher temperature, demonstrating a greater amount of deposited copper-containing compounds. This can be seen better on etched samples. The high-resolution spectra indicate that the binding energy values are 932.2–932.4 eV for the  $\text{Cu}2p_{3/2}$  region, which equates to  $\text{CuSe}$  (932.27 eV) [24],  $\text{CuInSe}_2$  (931.8–932.49 eV) [25],  $\text{Cu}_2\text{Se}$  (931.9–932.5 eV) [26], and  $\text{Cu}_2\text{O}$  (932.3–932.5 eV) [27,28]. The peaks at 952.2–952.4 eV found in the  $\text{Cu}2p_{1/2}$  region correspond to  $\text{CuInSe}_2$  (952.31 eV) [25] and  $\text{Cu}_2\text{O}$  (952.5 eV) [28]. The  $\text{In}3d_{5/2}$  spectra region has the peaks at 445.1–445.9 eV, and these binding energy values correspond to  $\text{In}_2\text{Se}_3$  (445.1 eV) [29],  $\text{In}(\text{OH})_3$  (445.0–445.2 eV) [30], and  $\text{InCl}_3$  (445.9 eV) [31]. The NIST XPS does not have any entries matching the  $\text{In}3d_{3/2}$  spectra region, making results inconclusive. All XPS spectra show that all the samples that were etched have more intense peaks than non-etched samples. This is especially noticeable in the peak values of  $\text{Cu}2p$  and, to a lesser degree,  $\text{In}3d$ . This suggests that the deeper films contain more Se, Cu, and In, while the surface of films contain more impurities, residues of salts, and oxides. The

full spectrum of XPS analysis revealed some impurity elements, O and Cl. The presence of oxygen can be explained by exposure to the atmosphere and the formation of oxides, as well as hydrolysis. The residual element Cl may come from the  $\text{InCl}_3$  precursor solution.

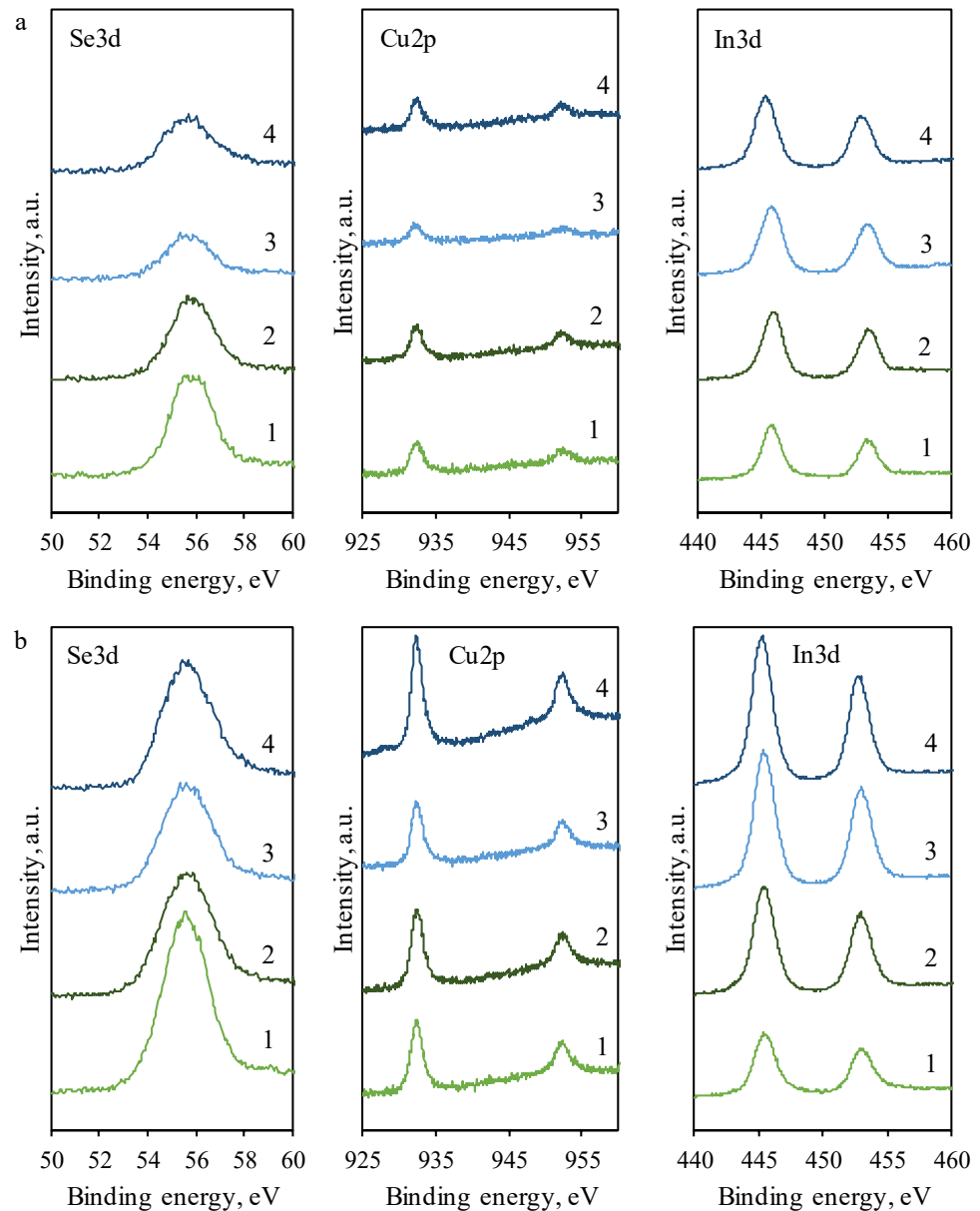


**Figure 3.** XPS spectra of In-incorporated  $\text{Cu}_x\text{Se}$  non-etched (a) and etched (b) films. Treatment with copper(II/I) ion solution: 1—10 min at 40 °C; 2—20 min at 40 °C; 3—5 min at 60 °C; and 4—10 min at 60 °C.

In our opinion,  $\text{Cu}_2\text{Se}$  could be formed on the surface due to a dense selenide film, which prevents the penetration of  $\text{Cu(I)}$  ions and interaction with elemental selenium. The formed  $\text{Cu}_x\text{Se}$  distinguishes the reacting substances ( $\text{Cu}^+$  and  $\text{Se}$ ) from one another, thus the subsequent formation process is only possible due to the diffusion of reactants through the selenide film. Consequently,  $\text{Cu}_2\text{Se}$  could form on the surface of the film. In a deeper layer, the formation of  $\text{CuSe}$  is possible due to the solid-phase reaction of copper selenide with selenium. Elemental selenium as an oxidizer and  $\text{Cu}_x\text{Se}$  react toward a decrease in the  $x$  value via reactions (6) and (7):





### 3.3. SEM/EDX Analysis

The color of the prepared films on the glass substrate changes from transparent to red during reaction (2), when the elemental selenium is deposited, and to a dark gray when copper selenide and indium-incorporated copper selenide films are formed (reactions (3)–(5)).

Structural features and surface morphology of the deposited films were analyzed using SEM, images from which are shown in Figure 4 graphs (a,b,c,d). Magnifications of 1000 (b,d) and 4000 (a,c) were used. The micrographs show a compact structure composed of single-type grains. The individual grains have a dendritic structure; grains are agglomerated and not well defined.

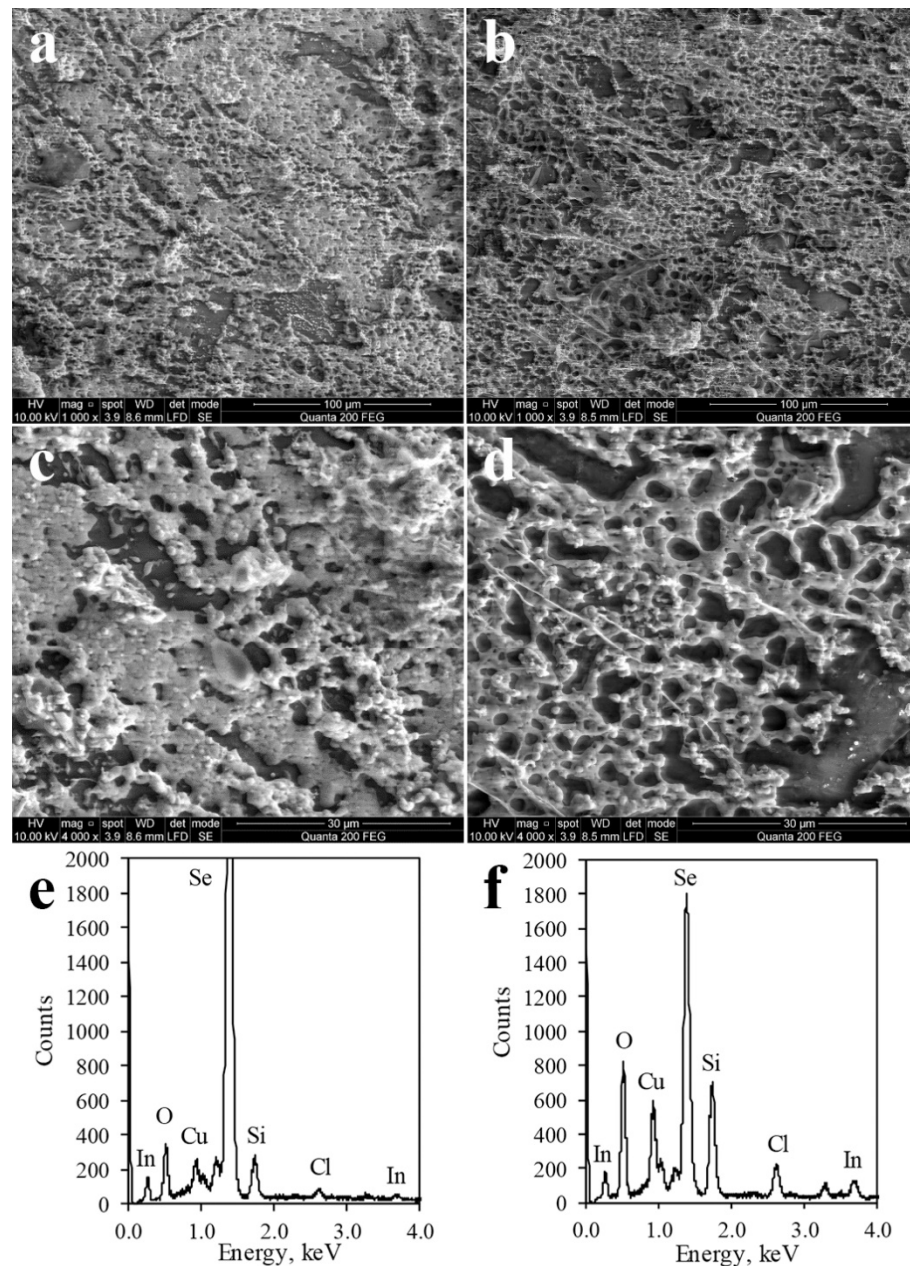


**Figure 4.** SEM images (a–d) and EDX spectra (e,f) of In-incorporated  $\text{Cu}_x\text{Se}$  film on glass. SEM images are 4000 $\times$  (a,c) and 1000 $\times$  (b,d) magnifications. Treatment with copper(II/I) ion solution: (a,c,e) 10 min at 40  $^\circ\text{C}$  and (b,d,f) 10 min at 60  $^\circ\text{C}$ .

EDX spectroscopy was used to study the elemental composition of obtained films. Peaks in EDX spectra shown in Figure 4 graphs (e,f) indicate atomic mass ratios of each element in the film. EDX spectra shows that the surface of the film, which was treated with copper(II/I) ion solution at a higher temperature (60 °C vs. 40 °C), contains more copper, a similar amount of indium, and less selenium. The lower peak of selenium could be explained by the formation of more copper containing compounds, such as  $\text{Cu}_{0.87}\text{Se}$  and  $\text{CuInSe}_2$ , due to a higher temperature and covering of elemental selenium. Besides selenium, copper, and indium, traces of other elements such as oxygen, chlorine, and silicon were found. The presence of oxygen may be explained by the dendritic film structure absorbing oxygen from the atmosphere. Silicon is part of the glass substrate itself, and the residual amount of chlorine may be brought in during the step of In-incorporation.

To estimate the thickness of In-incorporated copper selenide films, cross-section images were taken. The micrographs revealed the film size to be similar for all samples, about 90  $\mu\text{m}$  (Figure 5). It is possible that the temperature and duration of the initial deposition of selenium film determines the thickness of the film.

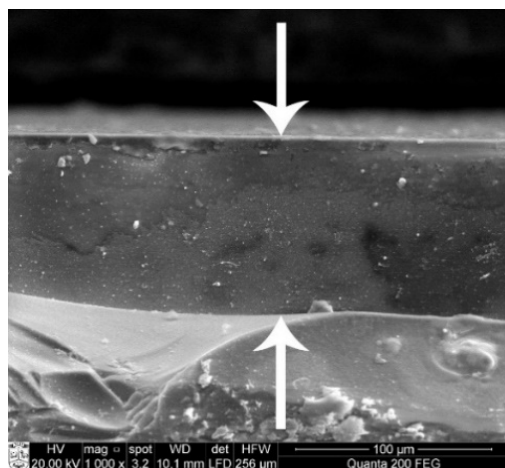


**Figure 5.** SEM cross-section image of In-incorporated  $\text{Cu}_x\text{Se}$  annealed film on glass. Treatment with copper(II/I) ion solution was 10 min at 60 °C.

### 3.4. AAS Analysis

The AAS analysis method was used to assess atomic amounts of Se, Cu, and In in obtained films. The data is shown in Table 1 and it coincides with the data obtained using the XRD, XPS, and EDX methods. All samples have similar amounts of selenium because all of the samples were deposited using the same selenization temperature and duration. The temperature and duration of the treatment with copper(II/I) ion solution have a major effect on the amounts of copper in the formed indium-incorporated copper selenide films. A longer treatment with copper ion solution and an increased temperature allows more copper to react with deposited elemental selenium, resulting in copper-rich films. The sample that was treated for 10 min at 40 °C had less copper than the 20 min one, additionally the sample treat for 5 min at 60 °C had less copper compared to the 10 min samples. Likewise, the 40 °C sample ( $0.50 \mu\text{mol}/\text{cm}^2$ ) had less copper than the 60 °C sample ( $0.78 \mu\text{mol}/\text{cm}^2$ ), both samples were treated for 10 min. The AAS analysis data lines up with the XRD data shown in Figure 2. A longer treatment with copper(II/I) ion solution at higher temperatures yields films with a larger amount of copper selenide (hexagonal klockmannite,  $\text{Cu}_{0.87}\text{Se}$ ), because the peaks are more intense. Furthermore, all samples have similar amounts of indium because of the same conditions of indium(III) incorporation.

**Table 1.** Amount of Cu, Se, and In in In- incorporated Cu<sub>x</sub>Se films on glass.

Copper(II/I) Ion Solution Treatment Conditions		Amount of Elements, $\mu\text{mol}/\text{cm}^2$		
Temperature, $^{\circ}\text{C}$	Duration, min	Cu	Se	In
40 $^{\circ}\text{C}$	10	0.50	2.86	0.26
	20	0.59	2.85	0.27
60 $^{\circ}\text{C}$	5	0.69	2.95	0.29
	10	0.78	2.89	0.32

### 3.5. Optical Properties

Optical transitions in semiconductors play an important role in their characterization. Optical properties were studied by measuring the absorption spectra of films and calculating the Tauc plot. It shows the energy of the light  $h\nu$  versus absorption quantity  $(\alpha h\nu)^n$ , where  $\alpha$  is the absorption coefficient of the studied film material. In order to calculate the energy bandgap ( $E_g$ ) of the obtained films the Tauc plot was used [32–34]:

$$\alpha = \left( \frac{A}{h\nu} \right) (h\nu - E_g)^n \quad (8)$$

where  $A$  is the parameter that depends on transition chance and  $n$  is the value that depends on transition type. The number  $n = 2$  denotes direct band gap transition and  $n = \frac{1}{2}$  denotes indirect band gap transition. The resulting plot has a distinct linear segment that indicates the beginning of the light absorption spectra. The intersection of the extrapolated linear part with the abscissa axis shows the band gap value  $E_g$ . Extrapolating the linear region to the abscissa yields the energy of the optical band gap of the material.

The band gap values of the prepared semiconductor films were found to be in a range of 1.28–1.48 eV. This corresponds to the absorption start at 840–970 nm. These band gap values are similar to the compounds identified by XPS and XRD analysis. The band gap values of various semiconductors are shown in Table 2.

**Table 2.** The band gap values of selenium, copper selenide, copper indium selenide, and indium selenide found in the literature.

Semiconductor Material	Band Gap $E_g$ , eV	Reference
Se	1.60 eV	[35]
CuSe	1.80–2.10 eV	[36]
Cu <sub>2-x</sub> Se	1.4–2.2 eV	[37]
Cu <sub>2</sub> Se	1.1–1.27 eV	[38]
CuInSe <sub>2</sub>	1.04 eV	
CuIn <sub>3</sub> Se <sub>5</sub>	1.17 eV	[39]
CuIn <sub>5</sub> Se <sub>8</sub>	1.22–1.24 eV	
In <sub>2</sub> Se <sub>3</sub>	1.55 eV	[40]

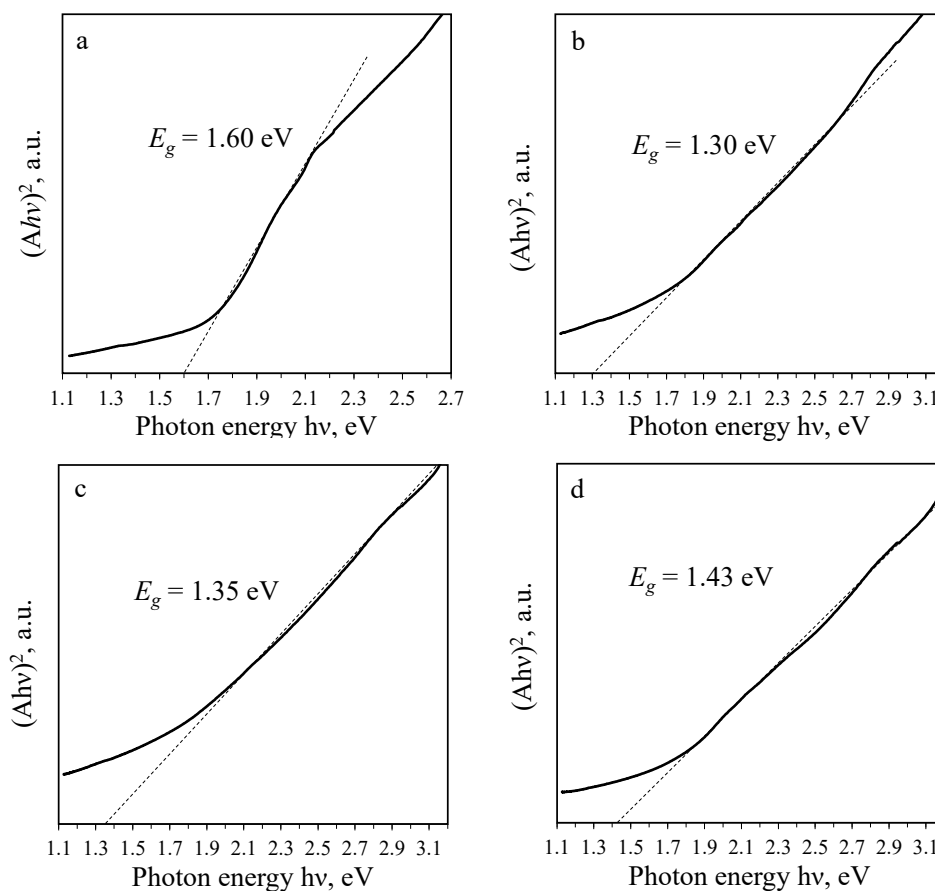


**Figure 6.** Tauc plot of obtained films on glass: (a) after selenization, (b) after treatment with copper(II/I) ion solution at 60 °C for 5 min, (c) after In-incorporation, and (d) after annealing.

#### 4. Conclusions

The SILAR method was successfully used to deposit  $\text{Cu}_x\text{Se}$  and In-incorporated  $\text{Cu}_x\text{Se}$  films. The aqueous solutions of  $\text{H}_2\text{Se}_n\text{S}_2\text{O}_6$ -type acids were suitable as a selenium precursor. The films were formed using three steps: the deposition of selenium film, the formation of copper selenide film, and the formation of indium–copper selenide film by incorporating and annealing. A number of phases were identified by XRD analysis: hexagonal klockmannite, cubic indium selenide, hexagonal selenium, indium selenide, and cubic copper indium selenide. A mixture of various compounds in the films was confirmed by XPS analysis. The SEM analysis showed that the films have a dendritic structure, agglomerated and not-well-defined grains, and a film thickness of  $\sim 90$   $\mu\text{m}$ . The AAS and EDX analyses showed that the films contained similar amounts of selenium and indium, while samples treated at a higher temperature and for a longer duration with the solution of copper(II/I) ions had more copper. The analysis of optical properties showed that the band gap values of copper selenide are 1.28–1.30 eV. The band gap values of indium-incorporated copper selenide increased by 5% (1.32–1.38 eV), and increased again by another 5% after annealing (1.42–1.48 eV). The optical properties of the formed films match the optical properties of copper selenide and indium selenide semiconductors.

**Author Contributions:** Conceptualization, A.I. and I.A.; methodology, A.I.; software, A.I.; validation, R.I.; formal analysis, A.I.; investigation, A.I.; resources, I.A. and R.I.; data curation, I.A.; writing—original draft preparation, A.I.; writing—review and editing, A.I. and R.I.; visualization, A.I.; supervision, I.A. All authors have read and agreed to the published version of the manuscript.

**Funding:** This research received no external funding.

**Institutional Review Board Statement:** Not applicable.

**Informed Consent Statement:** Not applicable.

**Data Availability Statement:** Not applicable.

**Conflicts of Interest:** The authors declare no conflict of interest.

## References

1. International Energy Agency (IEA). *Snapshot of Global Photovoltaic Markets*; Photovoltaic Power Systems Programme (PVPS): Paris, France, 2017; ISBN 978-3-906042-58-9.
2. Malaquias, J.C.; Steichen, M.; Thomassey, M.; Dale, P.J. Electrodeposition of Cu–In alloys from a choline chloride based deep eutectic solvent for photovoltaic applications. *Electrochim. Acta* **2013**, *103*, 15–22. [[CrossRef](#)]
3. Kashyout, A.E.; Ahmed, E.Z.; Meaz, T.; Nabil, M.; Amer, M. (One-step) electrochemical deposition and characterization of CuInSe<sub>2</sub> thin films. *Alex. Eng. J.* **2014**, *53*, 731–736. [[CrossRef](#)]
4. Tanaka, T.; Yamaguchi, T.; Ohshima, T.; Itoh, H.; Wakahara, A.; Yoshida, A. Effect of Cl ion implantation on electrical properties of CuInSe<sub>2</sub> thin films. *Sol. Energy Mater. Sol. Cells* **2003**, *75*, 109–113. [[CrossRef](#)]
5. Green, M.A.; Hishikawa, Y.; Dunlop, E.D.; Levi, D.H.; Hohl-Ebinger, J.; Yoshita, M.; Ho-Baillie, A.W.Y. Solar cell efficiency tables (Version 53). *Prog. Photovolt. Res. Appl.* **2019**, *27*, 3–12. [[CrossRef](#)]
6. Suzuki, T.; Ando, S. Preparation and Characterizations of CuInSe<sub>2</sub> Thin Films by Spin-Coating Method Using the Nanoparticles of CuInSe<sub>2</sub>. In Proceedings of the 2015 International Semiconductor Conference (CAS), Sinaia, Romania, 12–14 October 2015; IEEE: New York, NY, USA, 2015; pp. 81–84. [[CrossRef](#)]
7. Papadimitriou, D.; Roupakas, G.; Sáez-Araoz, R.; Lux-Steiner, M.-C.; Nickel, N.H.; Alamé, S.; Vogt, P.; Kneissl, M. Quality CuInSe<sub>2</sub> and Cu(In,Ga)Se<sub>2</sub> thin films processed by single-step electrochemical deposition techniques. *Mater. Res. Express* **2015**, *2*, 056402. [[CrossRef](#)]
8. Hankare, P.P.; Rathod, K.C.; Chate, P.; Jadhav, A.V.; Mulla, I.S. Preparation and characterization of CuInSe<sub>2</sub> thin films by chemical bath deposition technique. *J. Alloys Compd.* **2010**, *500*, 78–81. [[CrossRef](#)]
9. Islam, M.A.; Karim, A.M.M.T.; Julkarnain, M.; Badrul, A.K.M.; Khan, M.K.R.; Khan, K.A. Opto-transport properties of e-beam evaporated annealed CuInSe<sub>2</sub> thin films. *Surf. Interfaces* **2017**, *8*, 170–175. [[CrossRef](#)]
10. Yu, Z.; Yan, C.P.; Huang, T.; Huang, W.; Yan, Y.; Zhang, Y.X.; Liu, L.; Zhang, Y.X.; Zhao, Y. Influence of sputtering power on composition, structure and electrical properties of RF sputtered CuIn<sub>1-x</sub>Ga<sub>x</sub>Se<sub>2</sub> thin films. *Appl. Surf. Sci.* **2012**, *258*, 5222–5229. [[CrossRef](#)]
11. Thiru, S.; Asakawa, M.; Honda, K.; Kawaharazuka, A.; Tackeuchi, A.; Makimoto, T.; Horikoshi, Y. Study of single crystal CuInSe<sub>2</sub> thin films and CuGaSe<sub>2</sub>/CuInSe<sub>2</sub> single quantum well grown by molecular beam epitaxy. *J. Cryst. Growth* **2015**, *425*, 203–206. [[CrossRef](#)]
12. Zhou, J.; Zeng, Q.; Lv, D.; Sun, L.; Niu, L.; Fu, W.; Liu, F.; Shen, Z.; Jin, C.; Liu, Z. Controlled Synthesis of High-Quality Monolayered  $\alpha$ -In<sub>2</sub>Se<sub>3</sub> via Physical Vapor Deposition. *Nano Lett.* **2015**, *15*, 6400–6405. [[CrossRef](#)]
13. Zaghi, A.E.; Buffière, M.; Brammertz, G.; Lenaers, N.; Meuris, M.; Poortmans, J.; Vleugels, J. Selenization of printed Cu–In–Se alloy nanopowder layers for fabrication of CuInSe<sub>2</sub> thin film solar cells. *Thin Solid Films* **2015**, *582*, 18–22. [[CrossRef](#)]
14. Rahayu, S.U.; Lee, M.W. The investigation of chemically deposited Cu<sub>3</sub>BiS<sub>3</sub> into mesoporous TiO<sub>2</sub> films for the application of semiconductor-sensitized solar cells. In *Proceedings of the AIP Conference Proceedings*; American Institute of Physics Inc.: College Park, MD, USA, 31 March 2020; Volume 2221, p. 30005. [[CrossRef](#)]
15. Ashok, A.; Regmi, G.; Romero-Núñez, A.; Solis-López, M.; Velumani, S.; Castaneda, H. Comparative studies of CdS thin films by chemical bath deposition techniques as a buffer layer for solar cell applications. *J. Mater. Sci. Mater. Electron.* **2020**, *31*, 7499–7518. [[CrossRef](#)]
16. Lee, M.W. Sequential ionic layer adsorption reaction (SILAR)—A facile, low-cost growth method for ternary semiconductors for solar cells. In *Proceedings of the AIP Conference Proceedings*; American Institute of Physics Inc.: College Park, MD, USA, 31 March 2020; Volume 2221, p. 20003. [[CrossRef](#)]
17. Adeniji, Q.A.; Fowodu, T.O.; Odunaike, K.; Talabi, A.T. The growth and opto-electrical characterization of silar-grown iron copper sulphide (Fucus) ternary thin films. *Int. J. Thin Film Sci. Technol.* **2021**, *10*, 7–11. [[CrossRef](#)]
18. Kishore Kumar, D.; Loskot, J.; Kříž, J.; Bennett, N.; Upadhyaya, H.M.; Sadhu, V.; Venkata Reddy, C.; Reddy, K.R. Synthesis of SnSe quantum dots by successive ionic layer adsorption and reaction (SILAR) method for efficient solar cells applications. *Sol. Energy* **2020**, *199*, 570–574. [[CrossRef](#)]
19. Welegergs, G.G.; Gebretnisae, H.G.; Tsegay, M.G.; Nuru, Z.Y.; Dube, S.; Maaza, M. Thickness dependent morphological, structural and optical properties of SS/CuO nanocoatings as selective solar absorber. *Infrared Phys. Technol.* **2021**, *113*, 103619. [[CrossRef](#)]
20. Zelionkaitė, V.; Žarnauskas, A. The investigation of diffusion of interaction products between dilute. *Chem. Technol.* **2001**, *18*, 56–60.
21. Šukytė, J.; Ivanauskas, A.; Ancutienė, I. Comparative study of selenopolythionic acids H<sub>2</sub>Se<sub>n</sub>S<sub>2</sub>O<sub>6</sub> as precursors for formation of chalcogenides layers. In *Chemistry and Chemical Technology, Proceedings of the International Conference, Technologija, Kaunas, Lithuania*; Cambridge University Press: Cambridge, UK, 6 November 2014; pp. 124–127.
22. Haynes, W.M. *CRC Handbook of Chemistry and Physics*, 97th ed.; CRC Press: London, UK, 2016; ISBN 1498754287.

23. Malmsten, G.; Thorén, I.; Högberg, S.; Bergmark, J.-E.; Karlsson, S.-E.; Rebane, E. Selenium Compounds Studied by Means of ESCA. *Phys. Scr.* **1971**, *3*, 96–100. [[CrossRef](#)]
24. Yang, C.T.; Hsiang, H.I.; Tu, J.H. Copper selenide crystallites synthesized using the hot-injection process. *Adv. Powder Technol.* **2016**, *27*, 959–963. [[CrossRef](#)]
25. Sobol, P.E.; Nelson, A.J.; Schwerdtfeger, C.R.; Stickle, W.F.; Moulder, J.F. Single Crystal CuInSe<sub>2</sub> Analysis by High Resolution XPS. *Surf. Sci. Spectra* **1992**, *1*, 393. [[CrossRef](#)]
26. Cahen, D.; Ireland, P.J.; Kazmerski, L.L.; Thiel, F.A. X-ray photoelectron and Auger electron spectroscopic analysis of surface treatments and electrochemical decomposition of CuInSe<sub>2</sub> photoelectrodes. *J. Appl. Phys.* **1985**, *57*, 4761. [[CrossRef](#)]
27. Ertl, G.; Hierl, R.; Knözinger, H.; Thiele, N.; Urbach, H.P. XPS study of copper aluminate catalysts. *Appl. Surf. Sci.* **1980**, *5*, 49–64. [[CrossRef](#)]
28. Jolley, J.G.; Geesey, G.G.; Hankins, M.R.; Wright, R.B.; Wichlacz, P.L. Auger electron and X-ray photoelectron spectroscopic study of the biocorrosion of copper by alginic acid polysaccharide. *Appl. Surf. Sci.* **1989**, *37*, 469–480. [[CrossRef](#)]
29. Kazmerski, L.L.; Jamjoum, O.; Ireland, P.J.; Deb, S.K.; Mickelsen, R.A.; Chen, W. Initial oxidation of CuInSe<sub>2</sub>. *J. Vac. Sci. Technol.* **1981**, *19*, 467. [[CrossRef](#)]
30. Faur, M.; Faur, M.; Jayne, D.T.; Goradia, M.; Goradia, C. XPS investigation of anodic oxides grown on p-type InP. *Surf. Interface Anal.* **1990**, *15*, 641–650. [[CrossRef](#)]
31. Sakane, G.; Shibahara, T. Synthesis and characterization of the cubane-type molybdenum-indium mixed-metal cluster [Mo<sub>3</sub>InS<sub>4</sub>·2(H<sub>2</sub>O)<sub>10</sub>]<sup>3+</sup>. *Inorg. Chem.* **1993**, *32*, 777–778. [[CrossRef](#)]
32. Ghobadi, N.; Chobin, S.; Rezaee, S.; Shakoury, R. Tuning the optical and photocatalytic features of copper selenide prepared by chemical solution deposition method. *Surf. Interfaces* **2020**, *21*, 100706. [[CrossRef](#)]
33. Hashemi, M.; Bagher Ghorashi, S.M.; Tajabadi, F.; Taghavinia, N. Aqueous spray pyrolysis of CuInSe<sub>2</sub> thin films: Study of different indium salts in precursor solution on physical and electrical properties of sprayed thin films. *Mater. Sci. Semicond. Process.* **2021**, *126*, 105676. [[CrossRef](#)]
34. Ancutiene, I.; Bronusiene, A.; Baltrusaitis, J. Deposition and properties of mixed molybdenum sulfide (MoS<sub>2</sub>) and copper sulfide (Cu<sub>x</sub>S) films on glass surface using elemental sulfur as a precursor. *Thin Solid Films* **2020**, *709*, 138209. [[CrossRef](#)]
35. Gates, B.; Mayers, B.; Cattle, B.; Xia, Y. Synthesis and Characterization of Uniform Nanowires of Trigonal Selenium. *Adv. Funct. Mater.* **2002**, *12*, 219. [[CrossRef](#)]
36. Shitu, I.G.; Talib, Z.A.; Chi, J.L.Y.; Kechick, M.M.A.; Baqiah, H. Influence of tartaric acid concentration on structural and optical properties of CuSe nanoparticles synthesized via microwave assisted method. *Results Phys.* **2020**, *17*, 103041. [[CrossRef](#)]
37. Liu, Y.; Shen, S.; Zhang, J.; Zhong, W.; Huang, X. Cu<sub>2-x</sub>Se/CdS composite photocatalyst with enhanced visible light photocatalysis activity. *Appl. Surf. Sci.* **2019**, *478*, 762–769. [[CrossRef](#)]
38. Babu, N.S.; Abdul Khadar, M. Deposition of nanocrystal thin films of Cu<sub>2</sub>Se and their optical and electrical characterization. *Appl. Surf. Sci.* **2019**, *474*, 34–41. [[CrossRef](#)]
39. Maeda, T.; Gong, W.; Wada, T. Crystallographic and optical properties and band structures of CuInSe<sub>2</sub>, CuIn<sub>3</sub>Se<sub>5</sub>, and CuIn<sub>5</sub>Se<sub>8</sub> phases in Cu-poor Cu<sub>2</sub>Se–In<sub>2</sub>Se<sub>3</sub> pseudo-binary system. *Jpn. J. Appl. Phys.* **2016**, *55*, 04ES15. [[CrossRef](#)]
40. Almeida, G.; Dogan, S.; Bertoni, G.; Giannini, C.; Gaspari, R.; Perissinotto, S.; Krahne, R.; Ghosh, S.; Manna, L. Colloidal Monolayer β-In<sub>2</sub>Se<sub>3</sub> Nanosheets with High Photoresponsivity. *J. Am. Chem. Soc.* **2017**, *139*, 3005–3011. [[CrossRef](#)] [[PubMed](#)]